Correspondence to:
C. Wang,
cwang@scsio.ac.cn

A North-South Contrast of Subsurface Salinity Anomalies in the Northwestern Pacific From 2002 to 2013

Youfang Yan[1] (iD), **Lea Svendsen**[2] (iD), **Chunzai Wang**[1] (iD), **Noel Keenlyside**[2,3] (iD), **and Dazhi Xu**[4]

[1]State Key Laboratory of Tropical Oceanography, South China Sea Institute of Oceanology, Chinese Academy of Sciences, Guangzhou, China, [2]Geophysical Institute, University of Bergen, and Bjerknes Centre for Climate Research, Bergen, Norway, [3]Nansen Environmental and Remote Sensing Center and Bjerknes Centre for Climate Research, Bergen, Norway, [4]South China Sea Marine Prediction Center, State Oceanic Administration, Guangzhou, China

Abstract This paper finds a north-south contrast of subsurface salinity trend during 2002–2013 in the northwestern Pacific. Both Argo float data and long-term repeat hydrographic measurements along the 137°E section show that salinity anomalies along the isopycnals of 24.5–25.4 kg/m^3 exhibit a pronounced decreasing trend north of 15°N and an increasing trend south of 15°N. We perform a quantitative analysis based on satellite-derived data and a qualitative analysis that used a lower-order isopycnal salinity model that represents key balance terms (i.e., evaporation E, precipitation P, and wind forcing advection). Both of the analyses consistently show that the subsurface salinity anomalies in the north and south of 15°N are induced by different physical processes. Fresher surface waters in the northwestern subtropical outcrop region due to an excess freshwater supply (E − P < 0) contribute to the freshening of subsurface waters north of 15°N. In contrast, saltier surface waters in the northeastern subtropical subduction region induced by a deficit of freshwater (E − P > 0) and anomalous ocean circulation associated with the recent accelerated trade winds of the tropical Pacific cause the saltiness of subsurface waters south of 15°N. The results imply that the salinity north-south contrast may play an important role in changing ocean thermocline structure and upper ocean stratification in the northwestern Pacific.

Plain Language Summary Salinity, along with temperature and density, is a fundamental variable for seawater and can be considered as a tracer of ocean circulation. Additionally, as an important indicator of freshwater flux, salinity change is an essential measure of the hydrological cycle. The observations show a north-south contrast of salinity trends in the northwestern Pacific. This north-south contrast features will change upper ocean structure such as mixed layer depth and oceanic barrier layers and ocean heat budget in the northwest Pacific, thus affecting the tropical cyclone and climate variability.

1. Introduction

Salinity is a fundamental variable for seawater and can be considered as a tracer of ocean circulation (e.g., Fedorov et al., 2007; Heffner et al., 2008). Additionally, as an important indicator of freshwater flux, salinity change is an essential measure of the hydrological cycle (Boyer et al., 2007). Previous studies have shown that a significant freshening of surface waters has been detected in the western tropical Pacific since the 1950s (Cravatte et al., 2009; Delcroix et al., 2011). This freshening might be a consequence of an increase of the global hydrological cycle and a weakening of oceanic and atmospheric circulations (Chou et al., 2007; Cravatte et al., 2009; Vecchi & Soden, 2007).

However, a remarkable intensification of surface winds in the tropical Pacific has been observed since 2001 (England et al., 2014; Medhaug et al., 2017), which has led to a cooling of surface waters and an enhanced subsurface heat storage as well as rapid sea level rise in the western Pacific. However, because of the lack of salinity observations, the salinity variability (especially subsurface salinity variability) and its response to the recent intensification of surface winds in the tropical Pacific is still unclear.

Ocean salinity observations, in particular subsurface salinity observations, are recently made available from Argo profiling floats (Roemmich & Steering, 2009). The growth of Argo observations in terms of spatial-temporal coverage, combined with more than 50 years of repeating hydrographic observations along the 137°E section from the Japan Meteorological Agency, allows to resolve the subsurface salinity variability in the North Pacific (e.g., Li et al., 2012; Nagano et al. 2015; Nan et al., 2015; Ren & Riser, 2010; Sasaki et al., 2010; Yan et al., 2012, 2013, 2017). For instance, based on Argo salinity from 2001 to 2008, Sasaki

et al. (2010) found the salinity anomalies along the isopycnals were generated and subducted in the northeastern subtropical North Pacific (120–150°W), and these anomalies could then be advected southwestward to the western boundary and equatorial regions by the mean geostrophic current. Using Argo-based Grid Point Values of the Monthly Objective Analysis (MOAA GPV) data set, Li et al. (2012) and Kolodziejczyk and Gaillard (2012) also found that the pronounced salinity anomalies were generated in the outcrop areas of the northeastern subtropics and were advected to the western boundary and equatorial regions and then affected thermal variations in the equatorial Pacific.

Similarly, using Argo-observed salinity, Yan et al. (2013, 2017) and Nan et al. (2015) analyzed the subsurface salinity variability in the northwestern subtropical Pacific. Their results showed that the subsurface salinity variability in the northwestern subtropical Pacific exhibited a pronounced freshening trend. This freshening is remotely connected to the surface salinity anomalies in the northwestern subtropical outcrop region (30–35°N, 130–160°E) by subduction and thermocline advection. Based on 50-year-long observations along 137°E in the western North Pacific subtropical gyre, Oka et al. (2017) observed freshening trend and decadal salinity variability in the western North Pacific subtropical gyre and found this variability was originated in the winter mixed layer in the Kuroshio Extension region and was transmitted to 137°E 1–2 years later in association with the subduction and advection of subtropical mode water.

Although the salinity anomalies in the northwestern subtropical Pacific and their advected characteristics have been investigated by Yan et al. (2013, 2017), Nan et al. (2015), and Oka et al. (2017), variability of subsurface salinity in the northwestern tropical Pacific is still unclear, especially for the recent intensification of surface winds in the tropical Pacific. In addition, does the subsurface salinity variability in the northwestern tropical Pacific show a similar change to that in the northwestern subtropical Pacific? If not, what controls the different variations? The purpose of this paper is to answer these questions. The paper is organized as follows. Section 2 provides a description of the data used in this study. Section 3 presents the results, which include the main pattern of salinity variability in the northwestern Pacific and its dynamical mechanism. A summary is given in Section 4.

2. Data

The monthly mean 1° × 1° temperature and salinity fields, known as the MOAA GPV based mainly on Argo observations, were compiled by Hosoda et al. (2008). In this study, we used the updated MOAA GPV temperature and salinity for the period 2002–2013. The accuracies of temperature and salinity data of Argo floats are 0.005 °C and 0.01 psu, respectively (Hosoda et al., 2008). In addition, in situ observations by conductivity-temperature-depth along 137°E repeat hydrographic section provided by the Japan Meteorological Agency are also used. The ship-based hydrographic observation along the 137°E meridian across the western North Pacific from 34°N south of Japan to 3°N off New Guinea since 1967 for winter and since 1972 for summer has been providing an unprecedented body of periodical observation data covering more than 50 years. Temperature and salinity data from the section are widely used to clarify long-term changes of currents and water masses in relation to climate variability. Evaporation (E) from the Objectively Analyzed air-sea Fluxes project was provided by the Woods Hole Oceanographic Institution (Yu & Weller, 2007), while precipitation (P) came from the Global Precipitation Climatology Project. The 10-m winds from the European Centre for Medium-Range Weather Forecasts (ECMWF) are used, as are sea surface height and geostrophic velocity anomalies provided by Archiving Validation and Interpretation of Satellite Oceanographic Data on a 0.25° × 0.25° resolution, which were produced and distributed by the Copernicus Marine and Environment Monitoring Service (http://www.marine.copernicus.eu). In addition, the Ocean Surface Current Analysis of Real-time (OSCAR) near-surface ocean currents is used, which is generated by the Earth and Space Research. OSCAR near-surface ocean currents are derived using quasi-linear and steady-flow momentum equations (Bonjean & Lagerloef, 2002). The horizontal velocity is directly estimated from sea surface height, surface vector wind, and sea surface temperature. In order to study subduction mechanisms, we use the velocity outputs from an eddy-resolving Ocean General Circulation Model for the Earth Simulator (OFES; Sasaki et al., 2004). The OFES covers most of the oceans (75°S–75°N), with a horizontal resolution of 0.18° in longitude and latitude and 54 levels in the vertical direction. Here the monthly mean hindcast outputs from 2002 to 2013 were used. All data sets were interpolated to the same resolutions, and the anomaly in each month is defined as the deviation of climatologic mean over the period of 2002–2013.
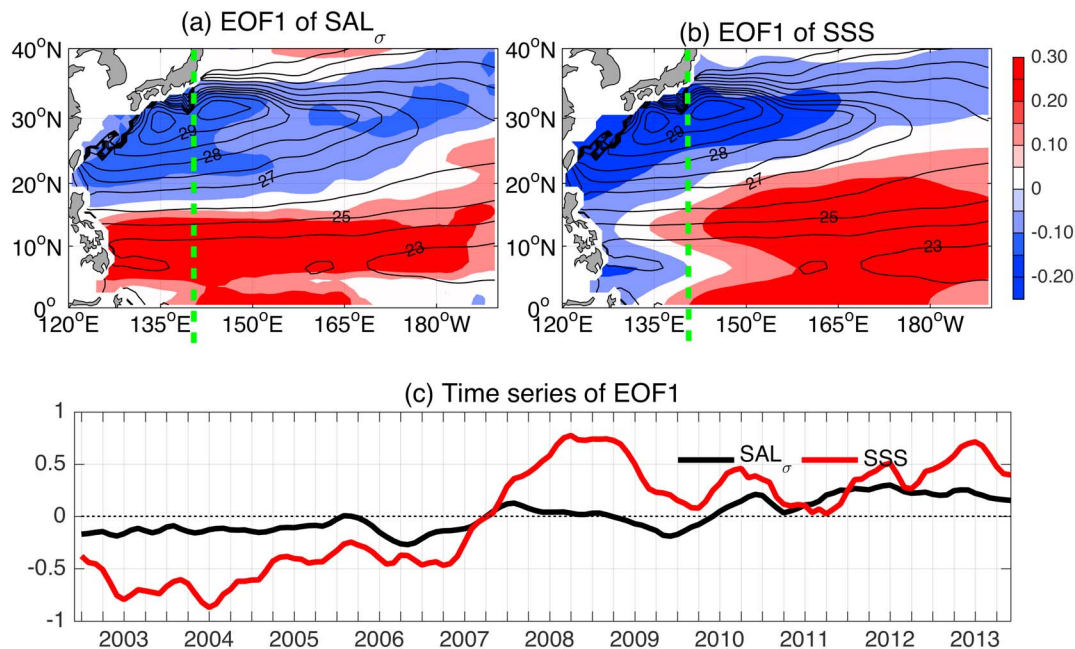
Figure 1. (a) The spatial patterns of the first empirical orthogonal function mode (EOF1; 53% of the variance) of salinity anomalies averaged over the 24.5- to 25.4-kg/m^3 isopycnals (SALσ); (b) same as (a) but for sea surface salinity (SSS) anomalies; and (c) the corresponding time coefficients of EOF1 for SALσ and SSS anomalies. The averaged isopycnals Montgomery geostrophic streamlines (in unit of m^2/s^2) over 24.5–25.4 kg/m^3 are shown by the black curves. The 137°E section is shown by the dashed green line.

Being a function of the ranks of the observations rather than their actual values, the Mann-Kendall trend test is not affected by the actual distribution of the data and is less sensitive to outliers. Thus, the Mann-Kendall test is more suitable for detecting significant trends in hydrological time series (Hamed & Rao, 1998) and is used for trend analysis in this study.

3. Results

3.1. North-South Contrast of Subsurface Salinity Anomalies

To investigate the temporal and spatial variability of salinity anomalies in the northwestern Pacific, we perform the empirical orthogonal function (EOF) analysis for salinity anomalies at the sea surface and at the subsurface. The subsurface of 24.5- to 25.4-kg/m^3 isopycnals, corresponding to ~50- to 100-m depth north of 15°N and ~150- to 300-m depth south of 15°N, is chosen because it is associated with a level of strong salinity variability and subduction (Nan et al., 2015; Yan et al., 2013; Yan et al., 2017). Figure 1 shows the first EOF (EOF1) of salinity anomalies and its corresponding time series. As shown in Figure 1a, the first EOF, which explains 53% of the total variance, exhibits a significant north-south contrast distribution with a negative sign north of 15°N and a positive sign south of 15°N. The corresponding time series shows an increasing trend from 2002 to 2013 (see black curve of Figure 1c), suggesting that the subsurface waters are getting fresher north of 15°N. This freshening is consistent with those of Li et al. (2012), Yan et al. (2013), Sugimoto et al. (2013), and Nan et al. (2015). On the contrary, south of 15°N, there is a saltier trend with subsurface salinity increasing from 2002 to 2013. This north-south contrasting trend is also found at the surface, but with freshening extending a little bit to the equator along the western boundary (Figures 1b and 1c).

To further illustrate this contrasting behavior, the linear trend of salinity anomalies along the meridional section of 137°E is also analyzed (Figure 2). The choice of the 137°E section is made because it is a repeat hydrographic observation section. In addition, it exactly passes through these contrasting regions (see Figure 1, green line). The surface waters become fresher north of 15°N, and this freshening further extends southward and penetrates to the deep ocean (Figure 2; see the blue contour). In the south, the waters become saltier in the upper ~300 m, with maximum increase at the subsurface (~150 m), in contrast to the maximum
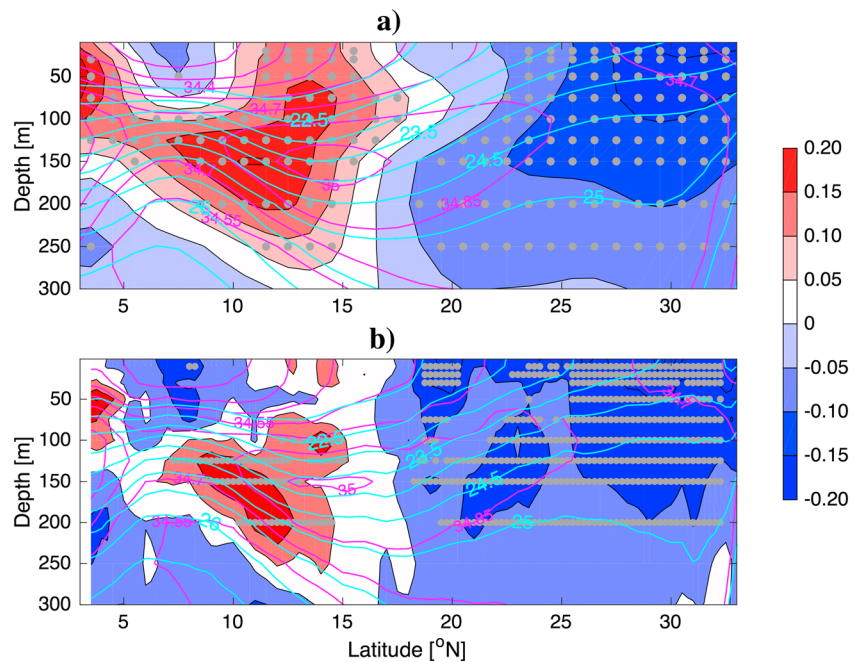
Figure 2. Linear trends (psu/10 years) of salinity anomalies along the 137°E section for (a) Argo-based Grid Point Values of the Monthly Objective Analysis and (b) the oceanographic observation obtained by Japan Meteorological Agency research vessels from 2002 to 2013. The climatological potential density and salinity are shown by the cyan and pink curves, respectively. The dots indicate that the trend is statistically significant at the 95% level.

freshening that occurs at the surface (Figure 2). This result is consistent with that of Figure 1 and indicates a robust north-south contrast of subsurface salinity trend in the northwestern Pacific.

### 3.2. Observed Causes of the North-South Contrast

What causes the prominent north-south contrast of subsurface salinity trend in the northwestern Pacific? To answer this question, we consider the factors that control the salinity distribution. In general, the salinity distribution in the ocean is influenced by evaporation, precipitation, isopycnal advection, eddy diffusion, and double diffusion (Bauer & Siedler, 1988). Because this study focuses on O (1,000 km) scale variations, the salinity variability due to eddy diffusion and double diffusion are not discussed although it may be large for submesoscale ocean processes. Thus, evaporation, precipitation, and the isopycnal advection are considered here.

Figure 3a shows the trends of evaporation (E) minus precipitation (P) and surface winds. During the period of 2002 to 2013, an excess freshwater supply (E − P < 0) was observed along the western boundary of the Pacific from 30°S to 30°N, including the South China Sea and eastern part of the Indian Ocean. In addition, an excess freshwater supply was also found in the southeastern Pacific and the northwestern subtropical Pacific (north of 15°N and west of 180°E; Figure 3a, shaded). In the rest of the Pacific, E − P did not exceed 0.2 cm/year, and a deficit of freshwater (E − P > 0) was seen in the tropical Pacific and the northeastern Pacific. This E − P trend pattern is consistent with that of sea surface salinity (SSS) anomalies (see Figure 1b) and that of freshwater forcing (Du et al., 2015), suggesting that air-sea freshwater exchange is indeed a dominant contributor for the SSS anomalies in the northwestern Pacific.

The subsurface salinity anomaly has also been changed in the northern Pacific, but its trend pattern does not match well with that of surface freshwater (see Figures 1a and 3a). The mismatching of surface freshwater (E − P) and the subsurface salinity trend implies the potential impact of ocean dynamics such as wind forcing and subduction processes. A careful examination of surface wind, which is closely related to ocean advection and subduction, showed that the surface wind in the Pacific increased substantially in both the tropics and the northeastern Pacific (Figures 3a and 4a, vectors). The increase of surface wind in the tropics
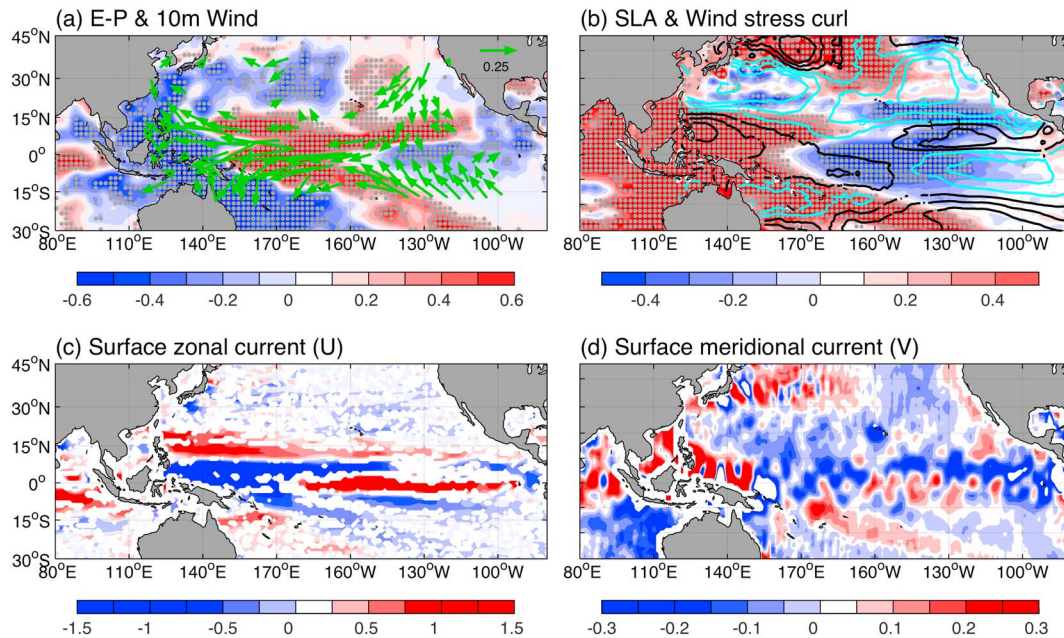
Figure 3. (a) Trends of E − P (cm/year) and surface wind (m·s^{-1}·year^{-1}; vectors); (b) trend of sea-level anomalies (SLAs; cm/year) and climatological mean of winter (December, January, and February) surface wind stress curl (N/m^3; contours) with positive and negative values in black and cyan curves, respectively; (c) trends of ocean surface zonal current (U, cm·s^{-1}·year^{-1}); and (d) meridional current (V, cm·s^{-1}·year^{-1}) from the Ocean Surface Current Analysis of Real-time (OSCAR) during 2002–2013. The regions with dots and vectors in (a) and (b) and the shaded regions in (c) and (d) are statistically significant at the 95% significance level.
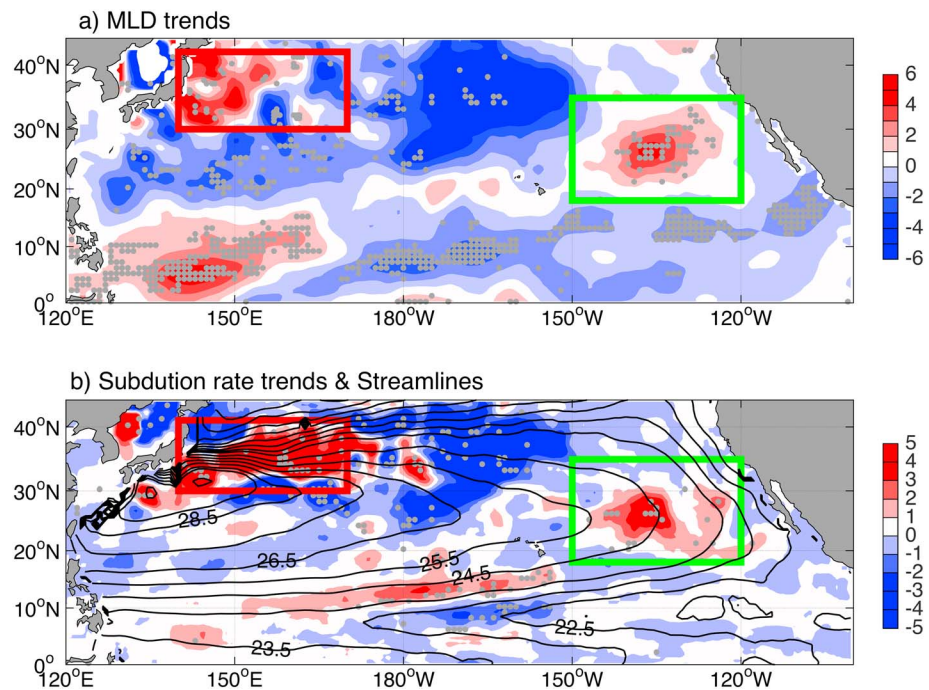
Figure 4. Trends of (a) mixed layer depth (MLD; m/year); and (b) subduction rate (m/year^2) and the Montgomery geostrophic streamfunction referred to 2,000 dbar (gray contours) along the 24.5- to 25.4-kg/m^3 isopycnals based on the Argo observations during 2002–2013. The annual subduction rate (R_{ann}), which is calculated by tracing water parcels released at the base of the winter mixed layer for 1 year in a Lagrangian framework, is expressed as: $R_{ann} = -\frac{1}{T} \int_{t1}^{t2} w_{mb} dt - \frac{1}{T} [h_m(t_2) - h_m(t_1)]$, where T represents the time period of integration; t_1 and t_2 are the end of the first and second winter, respectively; h_m is the MLD; and w_{mb} is the vertical velocity at the base of the mixed layer. The dots indicate that the trend is statistically significant at the 5% level. The subduction zones of the northeastern and northwestern subtropics are shown by the green box (18–30°N, 150–120°W) and red box (30–35°N, 130–160°E), respectively.
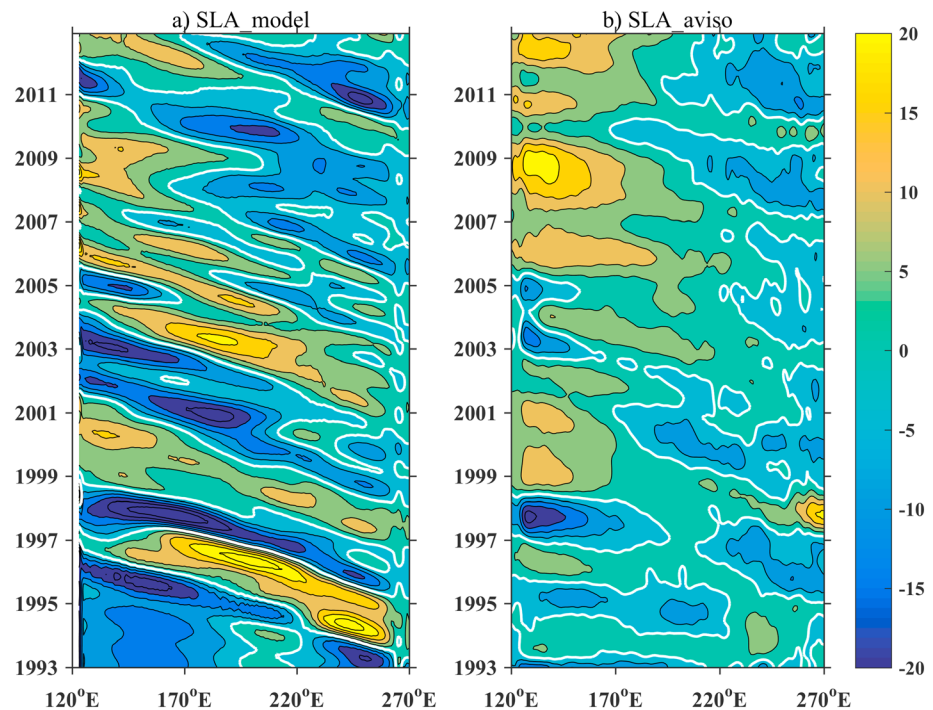
Figure 5. Time-longitude plot of sea-level anomalies (SLAs; cm) averaged along 13–14°N latitudinal band from (a) the 1½-layer reduced-gravity model and (b) from Archiving Validation and Interpretation of Satellite Oceanographic Data (AVISO) observations.

and the northeastern Pacific is consistent with that of England et al. (2014, their Figure 2a) and Du et al. (2015, their Figure 1d).

The increase of surface winds in the tropics leads to the changes of sea-level anomalies (SLAs; Figure 3b) and that of ocean circulation (Figures 3c and 3d). SLA drops in the eastern central Pacific but rises in the western Pacific. At the same time, there is an increase of eastward oceanic zonal flows in the tropical North Pacific (Figure 3c) at the sea surface, suggesting an acceleration of ocean circulation in the tropical Pacific.

The increase of tropical surface winds also drives the increase of mixed layer depth (MLD; Figure 5a) in the subduction zone of the northeastern subtropics (18–30°N, 150–120°W; green box) and northwestern tropics (0–10°N, 120–160°E). At the same time, a deeper MLD is also found in the northwestern subtropical subduction zone (30–35°N, 130–160°E; red box) although the local surface winds are not accelerated there (see Figure 3a). A change in the strength of subsurface stratification caused by a convoluted path of the Kuroshio Extension and by a shallowing of the main thermocline depth due to oceanic Rossby waves may be the main reason for the deeper MLD in this region, as suggested by Sugimoto and Kako (2016) who used observational data and simulation outputs from a one-dimensional turbulent closure model.

The deep MLD is favorable for the winter mixed layer waters to subduct into the thermocline (Qiu & Huang, 1995). The increasing MLD leads to higher rate of subduction in the northeastern and northwestern subtropical subduction regions (Figure 4b). The higher rate of subduction thus causes the fresher surface water in the northwestern subtropics (see Figure 3a) to subduct into the thermocline and be advected toward the eastern Luzon Strait along the southwestward thermocline pathway, as suggested by Yan et al. (2013, 2017) and Nan et al. (2015). This result is also consistent with that of Oka et al. (2017) who showed that the freshening trend and decadal salinity variability observed in the western North Pacific subtropical gyre were originated in the winter mixed layer in the Kuroshio Extension region and were transmitted to 137°E 1–2 years later in association with the subduction and advection of subtropical mode water. At the same time, the increase of MLD in the northeastern subtropics also favors an increase of subduction (Figure 4b), leading to saltier surface waters subducted here (see Figure 3a). These saltier waters are advected southwestward below the surface to the western boundary and equatorial regions along the mean geostrophic current (see also the

streamlines south of 10°N in Figure 4b), as suggested by Sasaki et al. (2010), Li et al. (2012), and Kolodziejczyk and Gaillard (2012).

In summary, the qualitative analyses suggested that SSS anomalies induced by anomalies of E – P and sea surface wind (and ocean circulation) during the period of 2002–2013 will contribute to the north-south contrast of subsurface salinity trends via two different southwestward thermocline pathways in the northern Pacific.

3.3. A Dynamical Explanation for the North-South Contrast

Following McDougall (1987) and Kilpatrick et al. (2011), salinity anomaly on a constant σ_θ isopycnal surface can be written as

$$\partial S'/\partial t + \overline{u}_{\sigma_\theta}\cdot\nabla_{\sigma_\theta}S' + u'_{\sigma_\theta}\cdot\nabla_{\sigma_\theta}\overline{S} = F_S' + \mathfrak{R} \tag{1}$$

where S', denoted with a prime, and $\overline{S}$, denoted with an overbar, are anomaly and climatologic mean of salinity, respectively; t is time; $\overline{u}_{\sigma_\theta}$ and u'_{σ_θ} are the climatological mean and anomaly of oceanic circulation along the isopycnal surface, respectively; $\nabla_{\sigma_\theta} = \frac{\partial}{\partial x} + \frac{\partial}{\partial y}$ is taken along σ_θ isopycnal surfaces; F_S' is the surface freshwater flux forcing; and $\mathfrak{R} = u'_{\sigma_\theta}\cdot\nabla_{\sigma_\theta}S' - \overline{u'_{\sigma_\theta}\cdot\nabla_{\sigma_\theta}S'}$. For the small and mesoscale eddies in the ocean, the salinity variance due to $\mathfrak{R}$ may be large and cannot be neglected. Because this study focuses on the scales of O (1,000 km), $\mathfrak{R}$ can be neglected when the subsurface salinity is calculated.

To evaluate the role of oceanic circulation variability in the salinity variability, we adopt in this study the 1½-layer reduced-gravity model that governs the baroclinic ocean response to surface wind forcing. This model has been used extensively in investigating the SLA or equivalently the upper ocean circulation variability in the tropical and midlatitude Pacific Ocean (e.g., Capotondi et al., 2003; Kessler, 1990; Qiu, 2003; White, 1977). The model dynamics are governed by the linear vorticity equation under the long-wave approximation

$$\frac{\partial\eta}{\partial t} - c_R\frac{\partial\eta}{\partial x} = \frac{g'}{\rho g}\nabla\times\left(\frac{\overrightarrow{\tau}}{f}\right) - \varepsilon\eta \tag{2}$$

where η is the SLA; $c_R = -\beta g' H/f^2$ is the speed of long baroclinic Rossby waves; x is the longitudinal coordinate, g' is the reduced gravity; ρ is the reference density; $\overrightarrow{\tau}$ is the wind stress; f is the Coriolis parameter; and ε is the Newtonian damping rate. Integrating equation (2) from the eastern boundary (x_e) along the baroclinic Rossby wave characteristic, we have (Qiu, 2003)

$$\begin{aligned}\eta(x,y,t) &= \eta\left(x_e,y,t-\frac{x-x_e}{c_R}\right)\exp\left[-\frac{\varepsilon(x-x_e)}{c_R}\right]\\&+\frac{g'}{\rho_0 g f c_R}\int_{x_e}^x \overrightarrow{k}\cdot\nabla\times\tau\left(x',y,t-\frac{x-x'}{c_R}\right)\exp\left[-\frac{\varepsilon(x-x')}{c_R}\right]dx'\end{aligned} \tag{3}$$

The first term on the right-hand side of (3) represents the influence of SLAs propagating from the eastern boundary as Rossby waves; the second term represents the sea surface height anomalies due to the surface wind forcing.

Since the first baroclinic mode dominates the large-scale geostrophic motion in the thermocline, the long-wavelength approximation is justified and the horizontal currents are in geostrophic balance (Qiu, 2003):

$$\overline{u'} = \frac{g}{f}\overrightarrow{k}\times\nabla\eta \tag{4}$$

Then equation (1) can be rewritten by replacing u' as

$$\partial S'_{adv}/\partial t + \overline{u}_{\sigma_\theta}\cdot\nabla_{\sigma_\theta}S'_{adv} = F_S' - \left(\frac{g}{f}\overrightarrow{k}\times\nabla\eta'\right)\cdot\nabla_{\sigma_\theta}\overline{S} \tag{5}$$

where $\overrightarrow{k}$ is the unit vector in the vertical direction; $F_S' = [SSSA(t-t_0) - dy\cdot|\nabla SSS|(t-t_0)]/dt$ with $dy = \frac{-SSD(t-t_0)-\overline{SSD(t-t_0)}}{|\nabla SSD(t-t_0)|}$. Here dy is the displacement of the isopycnal outcrop, which is frequently influenced by local heat and freshwater flux variability; t_0, the delay time, is defined as the advection time from
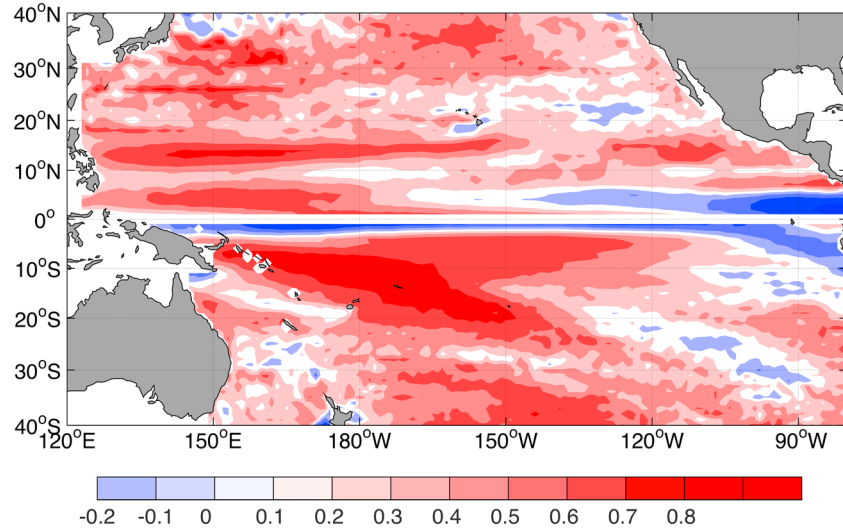
Figure 6. Point-to-point correlation coefficient between low-frequency (period >1 year) sea level from satellite observations and the 1½-layer reduced-gravity model during 1993–2013.

subduction to the focus region (Li et al., 2012; Oka et al., 2017; Sasaki et al., 2010; Yan et al., 2013, 2017), for example, 1–2 years for the region north of 15°N and 4–5 years south of 15°N; and *SSD* is the surface density.

The magnitude of SSS gradient is defined as $\nabla SSS = \sqrt{(\partial S/\partial x)^2 + (\partial S/\partial y)^2}$. Note that equation (5) only applies to long-wavelength variability generated in the thermocline away from the surface where u' includes higher-frequency Ekman currents. Then equation (5) can be rewritten as

$$\frac{\partial S'_{adv}}{\partial t} = \underbrace{F_S{}'}_{(SSSA\_forcing)} \underbrace{-\left(\frac{g}{f}\,\vec{k}\times\nabla\eta'\right)\cdot\nabla_{\sigma_\theta}\overline{S}}_{\left(U'_{adv}\_forcing\right)} \underbrace{-\overline{u}_{\sigma_\theta}\cdot\nabla_{\sigma_\theta}S'_{adv}}_{\left(\overline{u}_{adv}\_forcing\right)} \tag{6}$$
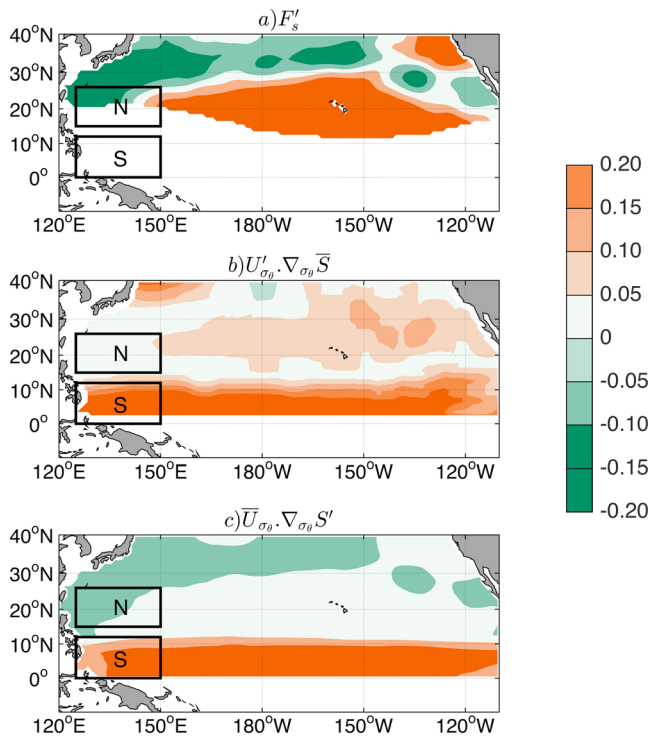
The first term on the right-hand side of equation (6) represents the influence of surface freshwater flux forcing ($F_S{}'$); the second and third terms represent the contribution of oceanic circulation anomalies (U'_{adv}_forcing) and ocean mean circulation ($\overline{U}_{adv}$ forcing) along the isopycnal surfaces.

Using equation (6), we can calculate the relative contribution of surface freshwater flux forcing and oceanic circulation anomalies to the salinity changes on the isopycnal surface. However, before doing this, we need to first assess the skill of equation (3) in describing variability in the focus region. In evaluating equation (3), we set $g' = 0.03$ m/s^2 (Qiu, 2003). The wave speed of the first baroclinic long Rossby wave (c_R) is calculated based on Chelton's first baroclinic Rossby radius of deformation data (Chelton et al., 1998). The dissipation rate ε is 1/(6 years) according to Qiu (2003). The eastern boundary sea level, $h(x_e, y, t)$, is determined by the monthly altimetric SLA in the grid cells closest to the eastern boundary. Wind stress curl is calculated using wind stress derived from ECMWF-Interim sea surface wind speed.

Figure 5 shows time-longitude diagrams of observed and modeled SLAs (period >1 year) averaged from 13°N to 14°N. Both observed and simulated SLAs show a westward extension. In addition to the good agreements near the eastern boundary, sea-level signals in the west are also similar to that of observation. Figure 6 shows the point-to-point correlation coefficients between sea level from satellite observations and 1½-layer reduced-gravity model during 2002–2013. Except the narrow bands located at the northeastern subtropical Pacific and tropical Pacific along ~0°N, correlations are positive and significant with $r > 0.4$, indicating the capability of the model to simulate large-scale and low-frequency sea-level fluctuations in the North Pacific.

The relative role of surface freshwater flux forcing ($F_S{}'$) and oceanic circulation (U'_{adv}_forcing and $\overline{U}_{adv}$ forcing) to the salinity variability along isopycnals is now quantitatively analyzed. From Figure 7a, we can see that the prominent negative $F_S{}'$ trends are shown in the subduction zone of the northwestern
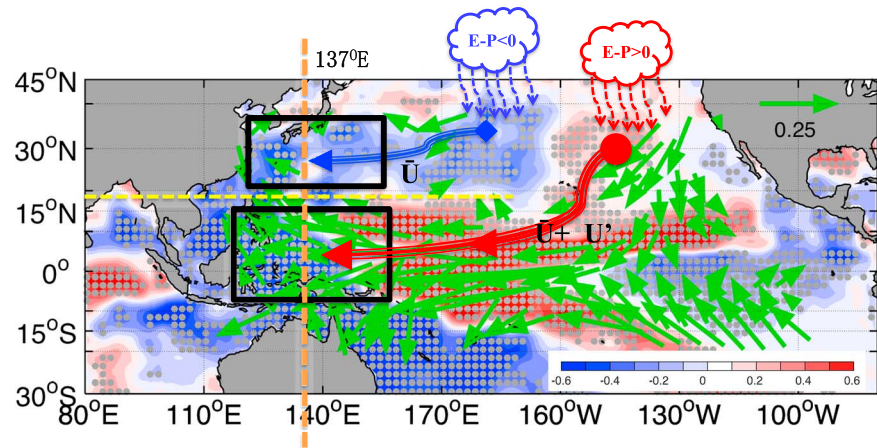
Figure 7. The trends of salinity anomalies induced by (a) sea surface salinity anomalies forcing (the first term on the right-hand side of equation (6)); (b) wind-induced ocean circulation anomalies forcing (the second term); and (c) ocean mean circulation forcing (the third term) along the isopycnal surfaces for the period of 2002–2013.

subtropics (25–30°N, 150–180°E), while positive F_S' trends are seen in the northeastern subtropics (18–30°N; 180–140°W). The largest positive salinity trends induced by $U'_{adv\_}$forcing ($U'_{\sigma_\theta}\cdot\nabla_{\sigma_\theta}\overline{S}$) occur in the tropical Pacific (south of ~10°N; Figure 7b). This region corresponds to the maximum acceleration of sea surface winds as found above (Figure 3a). Compared with that south of ~10°N, the salinity variability induced by $U'_{adv\_}$forcing ($U'_{\sigma_\theta}\cdot\nabla_{\sigma_\theta}\overline{S}$) in the region north of ~15°N is much smaller and almost equal to 0. These results are consistent with those of qualitative analyses (Figure 3a), implying that the surface wind anomalies play a significant (insignificant) impact on the subsurface water variability south (north) of ~15°N. Differing from that of wind anomalies, the salinity anomalies, which are advected by ocean mean circulation ($\overline{U}_{adv}$ forcing: $\overline{U}_{\sigma_\theta}\cdot\nabla_{\sigma_\theta}S'$), plays an important role in modulating the isopycnal salinity anomalies north of ~15°N (Figure 7c).

Because many previous studies have indicated that the surface salinity anomalies generated in the outcrop areas of the northeastern (northwestern) subtropics can be advected to the regions south (north) of 15°N via southwestward geostrophic current and then affect subsurface salinity variations by using the Hovmöllor diagram (e.g., Li et al., 2012; Sasaki et al., 2010; Yan et al., 2013, 2017), in this section, we only show the time variability of observed isopycnal salinity anomalies ($SALA_{\sigma_\theta}$) for the north (south) of 15°N (see box of N and S) and that of the simulated anomalous ocean circulation advection ($U'_{\sigma_\theta}\cdot\nabla_{\sigma_\theta}\overline{S}$) and mean oceanic circulation ($\overline{U}_{\sigma_\theta}\cdot\nabla_{\sigma_\theta}S'$) calculated along the paths of southwestward mean current (see Figure 9, Paths 1 and 2). In the regions north of 15°N (Figure 8a), the salinity anomaly induced by anomalous ocean circulation (Figure 8a, blue curve) is far smaller than that of observation (Figure 8a, black curve). Compared with that of anomalous ocean circulation, salinity anomalies
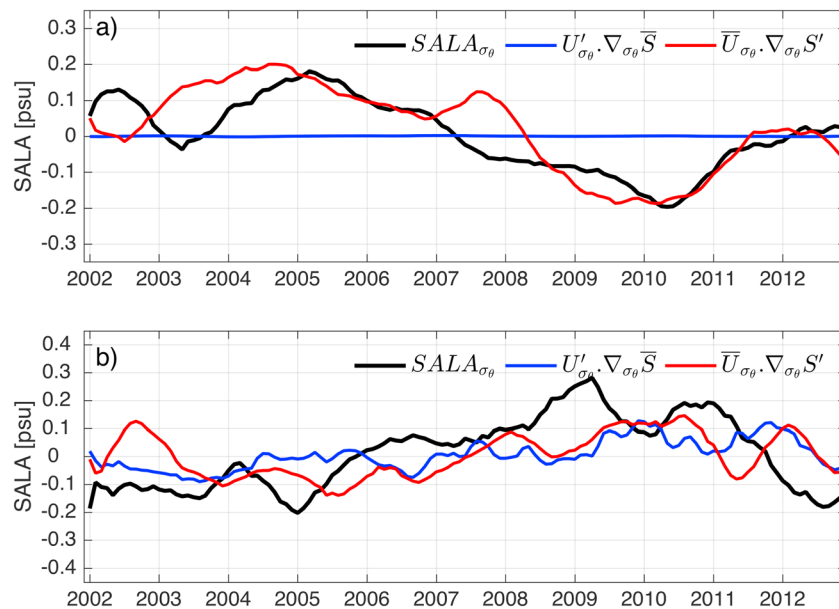
Figure 8. (a) The time variability of isopycnal salinity anomalies ($SALA_{\sigma_\theta}$; black line) for the box N, which is shown in Figure 7a, and that of anomalous ocean circulation advection ($U'_{\sigma_\theta}\cdot\nabla_{\sigma_\theta}\overline{S}$; blue line) and surface salinity anomalies in the subduction region advected by the mean oceanic circulation ($\overline{U}_{\sigma_\theta}\cdot\nabla_{\sigma_\theta}S'$; red line) along Path 2 (see Figure 9, blue arrow). (b) Same as (a) but for the box S along Path 1 (see Figure 9, red arrow).

Figure 9. Schematic diagram of physical processes that contribute to the subsurface salinity anomalies in the region north and south of 15°N. The contour represents the trends of E − P (cm/year); the vectors show the trends of surface wind (cm·s^{-1}·year^{-1}); the orange vertical dashed line shows the 137°E section; the horizontal yellow dashed line shows the boundary north and south of 15°N; and the colors denote the trend of E − P. The salinity anomalies in the northwestern (northeastern) subduction region were advected by the mean circulation along Path 2 in blue (Path 1 in red).

induced by the mean oceanic circulation (Figure 8a, red curve) are more larger with its magnitude almost equivalent to that of observations, although some discrepancy with observation is also shown. This result suggests that salinity anomalies induced by the mean oceanic circulation may be the dominant factor of the subsurface waters in the north of 15°N. In the region south of 15°N (Figure 8b), in addition to mean oceanic circulation contribution ($\overline{U}_{\sigma_\theta} \cdot \nabla_{\sigma_\theta} S'$; red line), the wind-induced ocean circulation anomalies ($U'_{\sigma_\theta} \cdot \nabla_{\sigma_\theta} \overline{S}$; blue line) also play an important role in the saltiness of subsurface water in the region south of 15°N.

4. Summary

The observations from Argo and the repeat hydrographic section along 137°E show a north-south contrast of salinity trend along the isopycnals of 24.5–25.4 kg/m^3 in the northwestern Pacific. The north-south contrast is characterized by the pronounced subsurface water freshening north of 15°N and saltiness south of 15°N.

Both qualitative and quantitative analyses suggest that the subsurface salinity anomalies north and south of 15°N are induced by different mechanisms. In the region north of 15°N, the freshening of subsurface water is mainly dominated by the salinity anomalies of the subduction region via mean ocean circulation. In the region south of 15°N, the subsurface salinity anomalies are not only related to saltier surface waters in the northeastern subtropical subduction region but also related to the ocean circulation anomalies induced by the recent acceleration of surface trade winds. As summarized in the schematic plot of Figure 9, anomalous freshening surface water, which was induced by an excess freshwater supply (E − P < 0) in the northwestern subtropical Pacific and was subducted and advected by mean ocean circulation ($\overline{U}$, blue arrow), contributed to the subsurface salinity freshening in the region north of 15°N. On the contrary, the saltier surface water was induced by a deficit of freshwater (E − P > 0) in the northeastern subtropics and was subducted and advected by a mean ocean circulation ($\overline{U}$, red arrow). This saltier water, combined with anomalous ocean circulation (U'), which was generated by the recent acceleration of surface trade winds during the period of 2002–2013, made contribution to the subsurface water saltiness in the region south of 15°N.

In summary, this paper finds a trend pattern of the north-south contrast of subsurface salinity in the northwestern Pacific and mechanisms for causing it. Since salinity variability in the western Pacific changes upper ocean structure such as MLD and oceanic barrier layer, it thus can affect ocean heat budget (Kolodziejczyk & Gaillard, 2012; Li et al., 2012). Further investigations of the north-south contrast of subsurface salinity anomalies and its possible relationships with ocean heat budget and tropical cyclones may help us improve the forecast of the tropical cyclone intensity in the northwest Pacific.

References

Bauer, E., & Siedler, G. (1988). The relative contributions of advection and isopycnal and diapycnal mixing below the subtropical salinity maximum. *Journal of Physical Oceanography*, 35, 811–837.

Bonjean, F., & Lagerloef, G. S. E. (2002). Diagnostic model and analysis of the surface currents in the tropical Pacific Ocean. *Journal of Physical Oceanography*, 32(10), 2938–2954. https://doi.org/10.1175/1520-0485(2002)032<2938:DMAAOT>2.0.CO;2

Boyer, T., Carton, J., Chao, Y., Gordon, A., Johnson, G., Lagerloef, G., et al. (2007). What's next for salinity? *Oceanography*, 21, 82–85.

Capotondi, A., Alexander, M. A., & Deser, C. (2003). Why are there Rossby wave maxima in the Pacific at 10°S and 13°N? *Journal of Physical Oceanography*, 33(8), 1549–1563. https://doi.org/10.1175/2407.1

Chelton, D. B., DeSzoeke, R. A., & Schlax, M. G. (1998). Geographical variability of the first baroclinic Rossby radius of deformation. *Journal of Physical Oceanography*, 28(3), 433–460. https://doi.org/10.1175/1520-0485(1998)028<0433:GVOTFB>2.0.CO;2

Chou, C., Tu, J. Y., & Tan, P. H. (2007). Asymmetry of tropical precipitation change under global warming. *Geophysical Research Letters*, 34, L17708. https://doi.org/10.1029/2007GL030327

Cravatte, S., Delcroix, T., Zhang, D., McPhaden, M., & Leloup, J. (2009). Observed freshening and warming of the western Pacifc warm pool. *Climate Dynamics*, 33(4), 565–589. https://doi.org/10.1007/s00382-009-0526-7

Delcroix, T., Alory, G., Cravatte, S., Corrège, T., & McPhaden, M. J. (2011). A gridded sea surface salinity data set for the tropical Pacific with sample applications (1950-2008). *Deep Sea Research*, 58(1), 38–48. https://doi.org/10.1016/j.dsr.2010.11.002

Du, Y., Zhang, Y., Feng, M., Wang, T., Zhang, N., & Wijffels, S. (2015). Decadal trends of the upper ocean salinity in the tropical indo-Pacific since mid-1990s. *Nature Scientific Reports*, 5(1605).

England, M. H., McGregor, S., Spence, P., Meehl, G. A., Timmermann, A., Cai, W., et al. (2014). Recent intensification of wind-driven circulation in the Pacific and the ongoing warming hiatus. *Nature Climate Change*, 4(3), 222–227. https://doi.org/10.1038/nclimate2106

Fedorov, A., Barreiro, M., Boccaletti, G., Pacanowski, R., & Philander, S. (2007). The freshening of surface waters in high latitudes: Effects on the thermohaline and wind-driven circulations. *Journal of Physical Oceanography*, 37(4), 896–907. https://doi.org/10.1175/JPO3033.1

Hamed, K. H., & Rao, A. R. (1998). A modified Mann-Kendall trend test for autocorrelated data. *Journal of Hydrology*, 204(1-4), 182–196. https://doi.org/10.1016/S0022-1694(97)00125-X

Heffner, D. M., Subrahmanyam, B., & Shriver, J. F. (2008). Indian Ocean Rossby waves detected in HYCOM sea surface salinity. *Geophysical Research Letters*, 35, L03605. https://doi.org/10.1029/2007GL032760

Hosoda, S., Ohira, T., & Nakamura, T. (2008). A monthly mean dataset of global oceanic temperature and salinity derived from Argo float observations. *JAMSTEC Report of Research and Development*, 8(0), 47–59. https://doi.org/10.5918/jamstecr.8.47

Kessler, W. S. (1990). Observation of long Rossby waves in the northern tropical Pacific. *Journal of Geophysical Research*, 95(C4), 5183–5217. https://doi.org/10.1029/JC095iC04p05183

Kilpatrick, T., Schneider, N., & Lorenzo, E. D. (2011). Generation of low-frequency spiciness variability in the thermocline. *Journal of Physical Oceanography*, 41(2), 365–377. https://doi.org/10.1175/2010JPO4443.1

Kolodziejczyk, N., & Gaillard, F. (2012). Observation of spiciness interannual variability in the Pacific pycnocline. *Journal of Geophysical Research*, 117, C12018. https://doi.org/10.1029/2012JC008365

Li, Y., Wang, F., & Sun, Y. (2012). Low-frequency spiciness variations in the tropical Pacific Ocean observed during 2003–2012. *Geophysical Research Letters*, 39, L23601. https://doi.org/10.1029/2012GL053971

McDougall, T. J. (1987). Neutral surfaces. *Journal of Physical Oceanography*, 17(11), 1950–1964. https://doi.org/10.1175/1520-0485(1987)017<1950:NS>2.0.CO;2

Medhaug, I., Stolpe, M. B., Fischer, E. M., & Knutti, R. (2017). Reconciling controversies about the 'global warming hiatus'. *Nature*, 545(7652), 41–47. https://doi.org/10.1038/nature22315

Nan, F., Yu, F., Xue, H., Wang, R., & Si, G. (2015). Ocean salinity changes in the Northwest Pacific subtropical gyre: The quasi-decadal oscillation and the freshening trend. *Journal of Geophysical Research: Oceans*, 120, 2179–2192. https://doi.org/10.1002/2014JC010536

Oka, E., Katsura, S., Inoue, H., Kojima, A., Kitamoto, M., Nakano, T., & Suga, T. (2017). Long-term change and variation of salinity in the western North Pacific subtropical gyre revealed by 50-year long observations along 137°E. *Journal of Oceanography*, 73(4), 479–490. https://doi.org/10.1007/s10872-017-0416-2

Qiu, B. (2003). Kuroshio extension variability and forcing of the Pacific decadal oscillations: Responses and potential feedback. *Journal of Physical Oceanography*, 33(12), 2465–2482. https://doi.org/10.1175/2459.1

Qiu, B., & Huang, R. X. (1995). Ventilation of the North Atlantic and North Pacific: Subduction versus obduction. *Journal of Physical Oceanography*, 25(10), 2374–2390. https://doi.org/10.1175/1520-0485(1995)025<2374:VOTNAA>2.0.CO;2

Ren, L., & Riser, S. C. (2010). Observations of decadal time scale salinity changes in the subtropical thermocline of the North Pacific Ocean. *Deep-Sea Research Part II-Topical Studies in Oceanography*, 57(13-14), 1161–1170. https://doi.org/10.1016/j.dsr2.2009.12.005

Roemmich, D., & Steering, T. A. (2009). Argo: The challenge of continuing 10 years of progress. *Oceanography*, 22(3), 46–55. https://doi.org/10.5670/oceanog.2009.65

Sasaki, H., Sasai, Y., Kawahara, S., Furuichi, M., Araki, F., Ishida, A., et al. (2004), A series of eddy-resolving ocean simulations in the world ocean: OFES (OGCM for the Earth simulator) project, in OCEAN 04, 3, 1535-1541, IEEE, https://doi.org/10.1029/2006GL028350

Sasaki, Y. N., Schneider, N., Maximenko, N., & Lebedev, K. (2010). Observational evidence for propagation of decadal spiciness anomalies in the North Pacific. *Geophysical Research Letters*, 37, L07708. https://doi.org/10.01029/02010GL042716

Sugimoto, S., & Kako, S. I. (2016). Decadal variations in wintertime mixed layer depth south of the Kuroshio Extension and its influence on winter mixed layer temperature. *Journal of Climate*, 29(3), 1237–1252. https://doi.org/10.1175/JCLI-D-15-0206.1

Sugimoto, S., Takahashi, N., & Hanawa, K. (2013). Marked freshening of North Pacific subtropical mode water in 2009 and 2010: Influence of freshwater supply in the 2008 warm season. *Geophysical Research Letters*, 40, 3102–3105. https://doi.org/10.1002/grl.50600

Vecchi, G. A., & Soden, B. J. (2007). Global warming and the weakening of the tropical circulation. *Journal of Climate*, 20(17), 4316–4340. https://doi.org/10.1175/JCLI4258.1

White, W. (1977). Annual forcing of baroclinic long waves in the tropical North Pacific Ocean. *Journal of Physical Oceanography*, 7(1), 50–61. https://doi.org/10.1175/1520-0485(1977)007<0050:AFOBLW>2.0.CO;2

Yan, Y., Chassignet, E. P., Qi, Y., & Dewar, W. K. (2013). Freshening of subsurface waters in the Northwest Pacific subtropical gyre: Observations and dynamics. *Journal of Physical Oceanography*, 43(12), 2733–2751. https://doi.org/10.1175/JPO-D-13-03.1

Yan, Y., Xu, D., Qi, Y., & Gan, Z. (2012). Observations of freshening in the Northwest Pacific subtropical gyre near Luzon Strait. *Atmosphere-Ocean*, 50(sup1), 92–102. https://doi.org/10.1080/07055900.07052012.07715078

Yan, Y., Xu, D., Yu, K., & Qi, Q. (2017). Propagation of the subsurface freshening water and its major source in the northwestern Pacific. *Journal of Geophysical Research: Oceans*, *122*, 6857–6871. https://doi.org/10.1002/2017JC013033

Yu, L., & Weller, R. A. (2007). Objectively analyzed air-sea heat fluxes for the global ice-free oceans (1981–2005). *Bulletin of the American Meteorological Society*, *88*(4), 527–540. https://doi.org/10.1175/BAMS-88-4-527